LOW-ORDER MODEL FOR THE LOW-FREQUENCY UNSTEADINESS IN OBLIQUE-SHOCK/TURBULENT-BOUNDARY-LAYER INTERACTIONS

Emile Touber
Department of Aeronautics
Imperial College London
South Kensington Campus, London SW7 2AZ, U.K.
e.touber@imperial.ac.uk

Neil D. Sandham
School of Engineering Sciences
University of Southampton
Southampton SO17 1BJ, U.K.
n.sandham@soton.ac.uk

ABSTRACT

The interaction between a turbulent supersonic boundary layer and an impinging shock wave is investigated numerically and analytically. The reflected-shock low-frequency motions are well captured even when using a narrow simulation domain, supporting the argument that one underlying key mechanism for the low-frequency shock motions is two dimensional. Based on a two-dimensional approach, a stochastic ordinary differential equation for the low-frequency coupling between the reflected shock and the boundary layer is obtained. The system is closed and applied to a wide range of input parameters. It is argued that the low-frequency shock motions are not necessarily a property of the forcing, either from upstream or downstream of the shock, but are simply an intrinsic property of the coupled dynamical system.

INTRODUCTION

The physical mechanisms at the origin of the observed low-frequency shock motions in shock wave/turbulent boundary layer interactions (SBLI) are not fully understood. A number of tentative explanations have been proposed, usually falling into one of two categories: the first relates the low-frequency motions to specific events or flow structures from the upstream turbulent boundary layer, whereas the second looks for causal mechanisms within the interaction itself (i.e. downstream of the shock). In both cases, the difficulty resides in identifying a mechanism that can span timescales of the order of $10^1\delta_0/\bar{u}_1$ to $10^2\delta_0/\bar{u}_1$, where δ_0 is the upstream boundary-layer 99% thickness and $\bar{u}_1$ the upstream freestream velocity.

The variety of the mechanisms proposed in the literature, together with the subsequent debate about the merits of one approach relative to another is symptomatic of the difficulty one has in identifying and then separating individual events from a (supposedly) non-linear (chaotic) system, where actual causal events may well be impossible to detect. Instead of reasoning about the relevance of one assumed mechanism against numerical/experimental data, an attempt to characterise in a useful way the properties of the dynamical system arising from the coupling between the shock and the boundary layer is sought.

The paper is organised as follows. The next section highlights the main steps for the derivation of a low-order model for the shock-foot low-frequency motions. Next, some implications of the model and its sensitivity to modelling errors are discussed.

A STOCHASTIC LOW-ORDER MODEL FOR THE SHOCK-FOOT MOTIONS

The momentum integral equation

Starting from the Navier–Stokes equations, and upon integrating the streamwise component of the momentum equation in the wall-normal direction (denoted y), one can derive a general form of the Momentum Integral Equation (MIE) where none of the classical assumptions (e.g. constant pressure in the wall-normal direction, steady state ...) are used. The resulting MIE is then expressed in the following moving coordinate system:

$$\xi \equiv \frac{x + l_0 - \varepsilon}{l_0 - \varepsilon + s} \tag{1}$$

where all notations are described in figure 1. Hence, in what follows, $\xi = 0$ is the instantaneous shock-foot position, ε the shock-foot displacement with respect to its mean position and $\xi = 1$ the instantaneous location of the shock crossing. Note that due to the presence of the boundary layer, the shock does not reach the wall and the foot is defined as the linear extension of the shock to the wall.

The following assumptions are made to simplify the

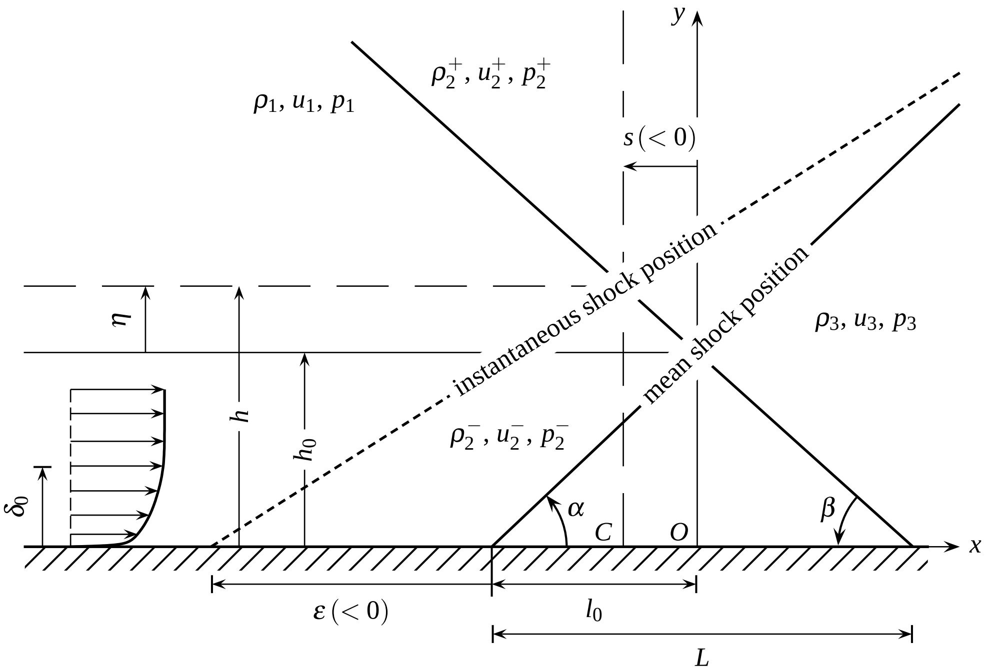

Figure 1: Sketch of the interaction with the definition of the notations in use

MIE:

1. the governing equation is written for $\xi < 1$
2. the potential flow is assumed constant (e.g. the acoustic field is neglected) so that u_1, ρ_1, and p_1 are true constants ($\rho_1 = \bar{\rho}_1$, $u_1 = \bar{u}_1$, $p_1 = \bar{p}_1$, where the overbar denotes time averaging)
3. the top boundary (delimited by h in figure 1) is assumed to be always inside the potential flow, i.e. $h > \delta_0$ at all times
4. the shock system is considered two-dimensional (i.e. spanwise variations are not considered) so that $h = h(t)$, $s = s(t)$, $\varepsilon = \varepsilon(t)$

Using the above assumptions, the MIE (expressed in the moving coordinate system) reads:

$$\frac{1}{u_1 l_0}\left[(1-\xi)\frac{\mathrm{d}\varepsilon}{\mathrm{d}t} + \xi\frac{\mathrm{d}s}{\mathrm{d}t}\right]\frac{\partial}{\partial \xi}\left[\delta_\rho - \delta_1\right] + \frac{1}{l_0}\frac{\partial \delta_2}{\partial \xi} + \frac{p_1}{\rho_1 u_1^2 l_0}\frac{\partial \delta_p}{\partial \xi} = \frac{1}{2}\left(1 - \frac{\varepsilon}{l_0} + \frac{s}{l_0}\right) C_f - \frac{1}{\rho_1 u_1^2 l_0 Re}\frac{\partial}{\partial \xi}\left[\int_0^h \tau_{xx}\mathrm{d}y\right] \quad (2)$$

where ρ_1, p_1 are the upstream freestream density and pressure, respectively (in this study, the temperature is related to the fluid density and pressure assuming the ideal-gas law to be applicable). The displacement, momentum, pressure and density thicknesses are defined (respectively):

$$\delta_1 = \int_0^h \left(1 - \frac{\rho u}{\rho_h u_h}\right)\mathrm{d}y \quad (3)$$

$$\delta_2 = \int_0^h \frac{\rho u}{\rho_h u_h}\left(1 - \frac{u}{u_h}\right)\mathrm{d}y \quad (4)$$

$$\delta_p = \int_0^h \left(1 - \frac{p}{p_h}\right)\mathrm{d}y \quad (5)$$

$$\delta_\rho = \int_0^h \left(1 - \frac{\rho}{\rho_h}\right)\mathrm{d}y \quad (6)$$

with ρ the fluid density, u the streamwise velocity component and p the pressure. Finally, C_f is the skin friction (i.e. $[2\mu_w/(Re\rho_h u_h^2)]\,\partial u/\partial y|_w$ with the subscript w denoting that the quantity is evaluated at the wall and μ is the dynamic viscosity), τ_{ij} is the usual viscous stress tensor and Re is the Reynolds number (i.e. $\rho_1 u_1 \ell/\mu_1$ with ℓ the reference scale used for x and y).

Similarity solution and reduced-order system

Starting from (2), a governing equation for ε is sought. To achieve this goal, the partial differential equation is transformed into an ordinary one by invoking the following hypothesis:

Hypothesis 1. *There exists a similarity function (F) that describes the streamwise evolution of the various boundary-layer thicknesses independent of the time variable, i.e.*

$$\begin{cases} F(\xi) \equiv \dfrac{\delta_i(\xi) - \delta_i(\xi = 0)}{\Delta_i} \\ \Delta_i(t) \equiv \delta_i(\xi = 1) - \delta_i(\xi = 0) \end{cases} \quad (7)$$

where the subscript i is any of the following: $1, 2, \rho, p$.

Mathematically, hypothesis 1 corresponds to the supposed existence of a separation of variables, an assumption which is reasonably well supported by simulation results (see Touber and Sandham, 2011). The MIE becomes:

$$\frac{1}{u_1 l_0}\left[(1-\xi)\frac{\mathrm{d}\varepsilon}{\mathrm{d}t}+\xi\frac{\mathrm{d}s}{\mathrm{d}t}\right]\left(F'\Delta_\rho - F'\Delta_1\right) + \frac{1}{l_0}F'\Delta_2 + \frac{p_1}{\rho_1 u_1^2 l_0}F'\Delta_p = \frac{1}{2}\left(1-\frac{\varepsilon}{l_0}+\frac{s}{l_0}\right)C_f \quad (8)$$

with $F' \equiv \mathrm{d}F/\mathrm{d}\xi$.

Next, (8) is evaluated at the shock foot ($\xi = 0$). Functions s, Δ_i and the slow-varying part of $C_f(\xi = 0)$ are expressed in terms of linear functions of ε. By retaining the leading-order terms only, a first-order stochastic ordinary differential equation (ODE) for the reflected-shock-foot motions is obtained (please see Touber and Sandham, 2011, for details), resembling the equation proposed by Plotkin (1975), who postulated that the shock displacement was obeying a first-order stochastic ODE with an associated characteristic timescale, which needs to be determined *a posteriori* from existing data. In the present work, an expression for the characteristic timescale is readily available.

Closed form of the system

After some modelling efforts, combined with series expansions of the shock-jump relations, the system is closed so that the following dynamical equation for the shock-foot motions may be written (see Touber and Sandham, 2011):

$$\frac{1}{\bar{u}_1}\frac{\mathrm{d}\varepsilon}{\mathrm{d}t}+\phi\frac{\varepsilon}{L}=\Pi C''_{f_0}(t) \quad (9)$$

with:

$$\Pi=\frac{\tan\beta}{2F'(0)\left(\tan\alpha+\tan\beta\right)} \quad (10)$$

$$\phi=\frac{2\gamma+\gamma(\gamma-1)\,\mathrm{M}_1^2}{(\gamma+1)\left[1+(1-r)P_2-rP_3\right]}\left\{\Pi\left[\left(\frac{1}{\tan\alpha}+\frac{1}{\tan\beta}\right)\left(\bar{C}_{f_0}-\Lambda\right)+\bar{C}_{f_0}\frac{\tan\alpha}{\tan\beta}\right]+\left(1-\frac{\tan\alpha\tan\beta}{\tan\alpha+\tan\beta}\right)\left[r''\frac{\gamma\mathrm{M}_1^2\bar{C}_{f_0}}{P_2-1}-r'D-r\frac{P_2\kappa}{\gamma+1}\left(\frac{\mathrm{M}_2}{\mathrm{M}_1}\right)^2\right]\right\} \quad (11)$$

$$\kappa=\frac{\tan\alpha+\tan\beta}{\tan\beta\left(1-1/\tan\alpha\right)-1}\sin(2\alpha)\sin\left[2(\alpha+\theta)\right] \quad (12)$$

$$D=\frac{\overline{\mathrm{M}}_3}{\mathrm{M}_1}\left\{\left(\frac{1}{2}\sqrt{\frac{R_3}{P_3}}-\frac{\overline{\mathrm{M}}_3}{\mathrm{M}_1}\right)A+\frac{1}{2}\sqrt{\frac{P_3}{R_3}}B+\left(\frac{\mathrm{M}_1}{\overline{\overline{\mathrm{M}}}_3}\sqrt{R_3P_3}-2P_3\right)C\right\} \quad (13)$$

$$A=\frac{\gamma\kappa\mathrm{M}_2^2}{1+\gamma}P_2 \quad (14)$$

$$B=\kappa R_3\left[\frac{1}{2\sin^2(\alpha+\theta)}-\frac{(\gamma-1)\,\mathrm{M}_2^2}{4+2(\gamma-1)\,\mathrm{M}_2^2\sin^2(\alpha+\theta)}\right] \quad (15)$$

$$C=\frac{\overline{\mathrm{M}}_3}{\mathrm{M}_1}\left\{\kappa\left[\frac{(\gamma-1)\,\mathrm{M}_2^2}{8+4(\gamma-1)\,\mathrm{M}_2^2\sin^2(\alpha+\theta)}-\frac{\gamma\mathrm{M}_2^2}{2(1-\gamma)+4\gamma\mathrm{M}_2^2\sin^2(\alpha+\theta)}\right]-\frac{(\tan\alpha+\tan\beta)\cos^2\alpha}{\tan\beta\left(1-1/\tan\alpha\right)-1}\right\} \quad (16)$$

where α, β, $P_2 \equiv p_2^+/p_1$, $P_3 \equiv \bar{p}_3/p_1$, $R_3 \equiv \bar{\rho}_3/\rho_1$, M_2 and $\overline{\mathrm{M}}_3$ are computed from the inviscid shock reflection problem for a given pair of wedge angle θ and upstream Mach number M_1. Factors $F'(0)$, r, r' and r'' are assumed to take the values of 0.12, 0.2, −0.14 and 0.2, respectively. Term $\bar{C}_{f_0}$ is an input parameter, together with the upstream Mach number M_1 and wedge angle θ. The coefficient Λ, although of the same order as $\bar{C}_{f_0}$, is not an input parameter and is not generally known. In this work, it is taken to be 3×10^{-3} (based on simulation data). The term C''_{f_0} corresponds to the skin-friction turbulence-related variations at the reflected-shock foot and therefore constitutes the dynamical-system input signal.

Equation (9) is a first-order linear stochastic differential equation resembling the Langevin equation for Brownian motion. It is possible to show that the autocorrelation function of the shock-foot motions in response to a white-noise forcing with amplitude $2q$ is an exponential if computed after the initial transients from starting up the flow (see Touber and Sandham, 2011, for details). Therefore, the Power Spectral Density function (PSD), which is the Fourier transform of the autocorrelation function, may be explicitly written:

$$\mathscr{S}(S_t)=\frac{A_0}{1+\left(S_t/\phi_{\max}\right)^2} \quad (17)$$

where $A_0 \equiv q\left[L/(\bar{u}_1\phi)\right]^2$, $\phi_{\max} \equiv \phi/(2\pi)$ and S_t is the Strouhal number ($S_t = fL/\bar{u}_1$). The PSD being more easily given for the wall pressure, the above expression which is valid for the shock-foot motions may be converted to wall pressure at the shock foot using:

$$\mathscr{S}_p(S_t)\approx\frac{A_0\left(\mathrm{d}\bar{p}_w/\mathrm{d}x|_{\bar{x}_0}\right)^2}{1+\left(S_t/\phi_{\max}\right)^2} \quad (18)$$

where $\mathrm{d}\bar{p}_w/\mathrm{d}x|_{\bar{x}_0}$ is the mean wall-pressure gradient at the mean shock-foot position.

IMPLICATIONS AND SENSITIVITY OF THE MODEL

First, the model is tested against both the experimental and simulation results for the 8-degree shock-reflection configuration of Dupont et al. (2006), as shown in figure 2. Both

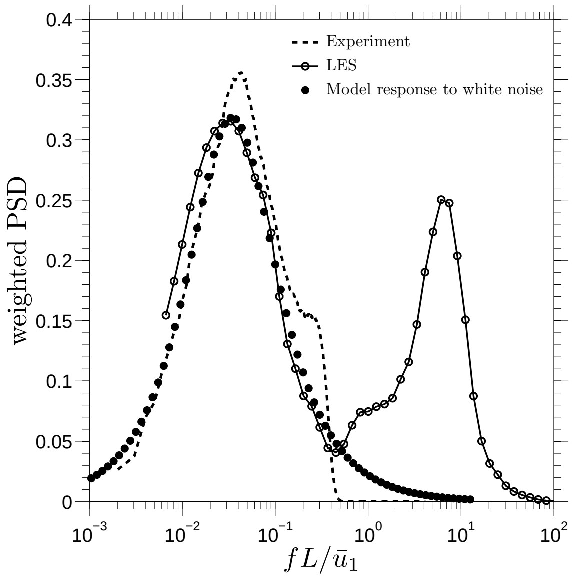

Figure 2: Premultiplied wall-pressure power-spectral-density distributions at the reflected-shock foot: model, large-eddy simulation (LES) and experimental results. The LES spectrum is taken from figure 17 in Touber and Sandham (2009) and the experimental data from Dupont et al. (2006)

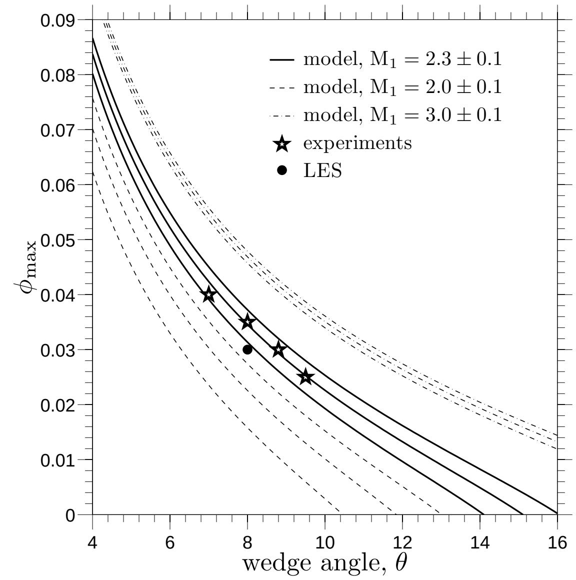

Figure 3: Predicted Strouhal-number value $\phi_{\max} \equiv f_{\max} L/\bar{u}_1$ of the most energetic shock oscillations (at frequency $f_{\max}$) for different upstream Mach numbers M_1 and wedge angles θ. Experimental and LES data are from Dupont et al. (2006) and Touber and Sandham (2009), respectively. For all cases, a variation of ± 0.1 in the upstream Mach number value is applied. Upstream skin-friction levels are the same as in Dupont et al. (2006)

the broadband nature and the frequency of the most energetic low-frequency pressure fluctuations in the vicinity of the shock foot location are reasonably well predicted.

The fundamental property of the shock/boundary-layer system indicated by (18) is its low-pass filter behaviour. As such, a transfer of energy from higher (turbulence-related) to lower frequencies is not required to explain the spectra in figure 2. Instead, the shock/boundary-layer system simply damps fluctuations greater than the cutoff frequency $\phi_{\max}$ while any existing fluctuations smaller than this cutoff frequency are amplified.

The use of white noise to force (9) may not seem ideal, as this is not, *a priori*, representative of turbulence fluctuations. However, it is argued that at low frequencies, skin-friction fluctuations solely associated with the contribution from the turbulence resembles that of a white noise, i.e. the spectrum of $C''_{f_0}(t)$ is "flat" at low frequencies, where (9) is to be applied.

One great advantage of the model is the possibility to use it for any given values of M_1 and θ. For a constant wedge angle, $\phi_{\max}$ increases with increasing Mach number and for a constant upstream Mach number, $\phi_{\max}$ decreases with increasing wedge angle. The latter trend can be tested against the experimental results of Dupont et al. (2006), as shown in figure 3. The agreement is well within the model and measurement uncertainties. Figure 4a shows the map of $\phi_{\max}$ for M_1 ranging from 1 to 6 and θ from 2° to 30°, whenever a regular reflection exists. Most values are within the range 10^{-2} to 10^{-1}, which is consistent with the experimental observations of SBLI (see Dussauge et al., 2006).

Although the final model is described by a linear equation, it does not mean that none of the non-linearities of the coupled shock/boundary-layer system are accounted for. Significant non-linear effects are mechanically embedded in the timescale ϕ^{-1}. Looking at the constituents of ϕ, one can see that even if the model is expressed in the form of point-particle dynamics (i.e. the shock-foot position), it does not convey a direct relation between a given velocity fluctuation and the shock response to it, as linearised Euler would do (the resulting spectrum would then be similar to the forcing), but instead it accounts for integrated effects by means of the different thicknesses which are non-linear functions of the velocity perturbations.

As discussed earlier, the model describes the coupled shock/boundary-layer system as a low-pass filter with characteristic timescale $\tau_s \sim \phi^{-1}$. One remarkable result is that this timescale is significantly larger than any characteristic timescales of the incoming boundary layer ($\phi/(2\pi)$ is in the 10^{-2} to 10^{-1} range giving $\tau_s \sim 10$ to $100L/\bar{u}_1$, to compare with $\delta_0/\bar{u}_1 \sim L/\bar{u}_1$, assuming that the interaction length scales with δ_0). This conforms to experimental observations (e.g. Dupont et al., 2006), and the known issue in numerical simulations that such flows have long initial transients, even for laminar cases (indeed, in the absence of forcing, the convergence to the steady solution would be as $\exp(-t/\tau_s)$).

The low-pass filtering property of the system indicates that, strictly speaking no transfer of energy from the higher to the lower frequencies is occurring. Instead, any high frequency is damped and any low frequency is amplified, with the frontier between high and low being determined by ϕ. Therefore, the system itself is simply amplifying *existing* low-frequency fluctuations, even if energetically insignificant, while it filters out any high-frequency content. Moreover,

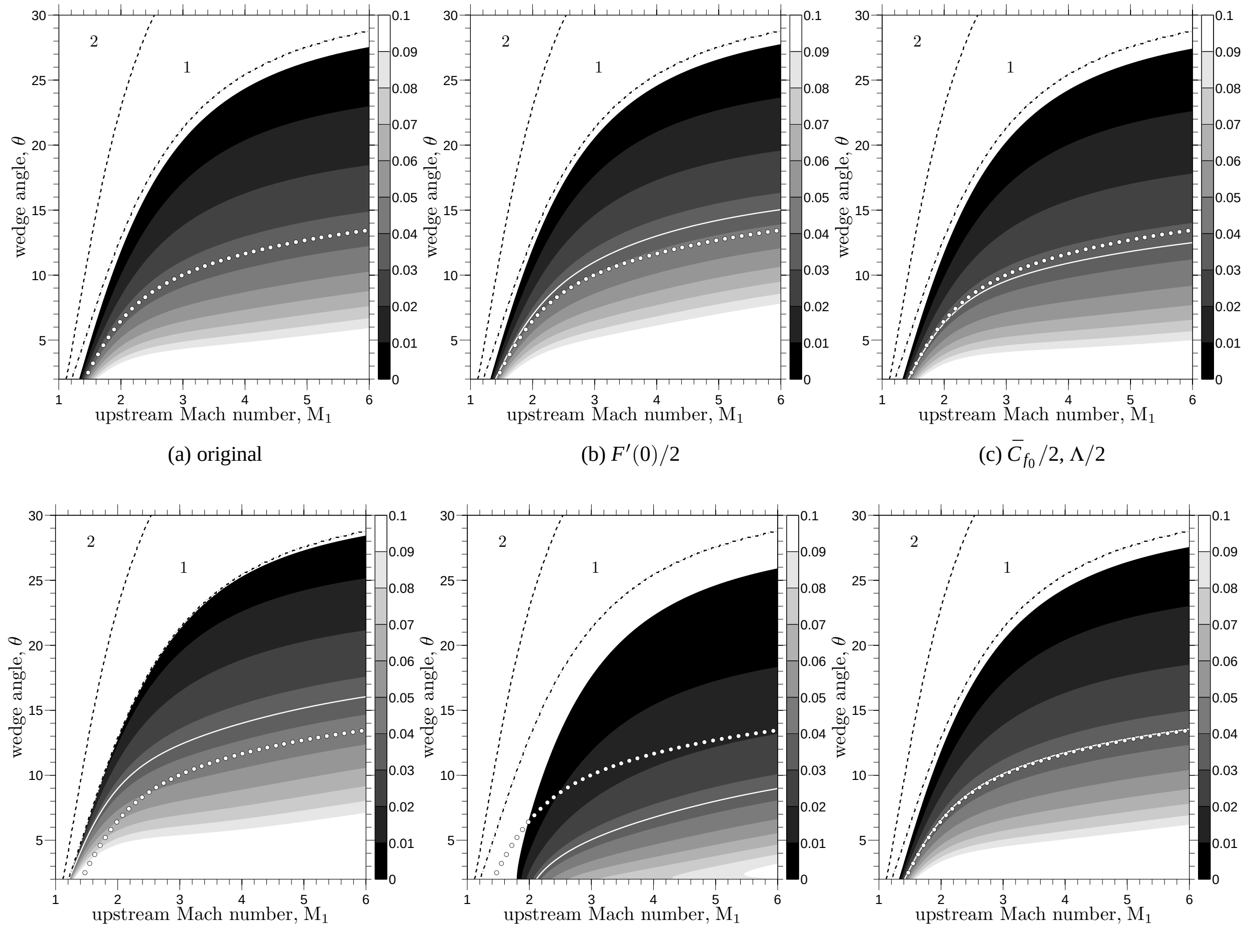

(a) original

(b) $F'(0)/2$

(c) $\bar{C}_{f_0}/2$, $\Lambda/2$

(d) $r/2$

(e) $r'/2$

(f) $r''/2$

Figure 4: Predicted most energetic low frequency $\phi_{\max}$ for different (M_1, θ) pairs and sensitivity to variations in the model constants. The *solid white line* gives the $\phi_{\max} = 0.035$ contour. The *dashed line* and *dash-dotted line* delimit two regions, labelled 1 and 2. Region 1 corresponds to Mach reflection cases and region 2 to cases where no oblique incident shock is formed. *White dots* indicate the position of the $\phi_{\max} = 0.035$ contour when using the reference values of (a)

the resulting broadband spectrum about a particular Strouhal number is not a property of the forcing but a characteristic of the shock/boundary-layer system itself (figure 2).

Based on the preceding discussion, it is inferred that the origin of the low-frequency oscillations is not in the forcing but in the dynamics of the system formed by the shock/boundary-layer interaction. Of course, if one applies any specific forcing below the natural frequency of the system, such forcing will be picked up and magnified. A specific forcing could be any significantly-long upstream coherent structures (see Ganapathisubramani et al., 2007, and references therein) or particular flow features within the interaction itself (see Dussauge and Piponniau, 2008; Piponniau et al., 2009; Pirozzoli and Grasso, 2006, and references therein). However, we stress that, mathematically speaking, these are not necessary and the low-frequency motions can simply arise from a background (white) noise, as successfully demonstrated in figure 2.

The robustness of the model to modelling errors is partially investigated in figure 4. First, the sensitivity of the model to the mean boundary-layer properties is weak for $\bar{C}_{f_0}$ and insignificant for r'', suggesting that the map in figure figure 4a is a good estimate for other mean boundary-layer properties (as long as the hypotheses used to derive the model hold). The mean boundary-layer properties thus play a major role in setting the interaction length (see the steady-state equation in Touber and Sandham, 2011) but their effect on the final dynamical equation is only weak. Second, the accuracy of the model for Δ_2 and to a lesser extent for Δ_p is crucial. While r can be easily determined to a relatively good accuracy, r' is the most critical aspect of the present model and further improvements could be sought in the future. Nevertheless, the overall monotonicity of the map of $\phi_{\max}$ and the order of magnitude of the predicted $\phi_{\max}$ are maintained even for these sensitive cases. This demonstrates that the Strouhal-number value for the most energetic low-frequency shock motions is robust with values remaining below 0.1 for a wide range of configurations, as argued by Dussauge et al. (2006).

Finally, it is important to bear in mind that the model is based on an approximate form of the momentum integral equation which itself relies on four assumptions (see earlier section), among which two are of primary importance. First, the interaction must be sufficiently large for the shock-crossing point to be above the incoming boundary layer. Therefore, one does not expect the model to be correct for weak interactions (i.e. for the smallest $(p_2^+ - p_1)/\tau_w$ values). Second, the interaction was considered to be two dimensional. Thus, any large spanwise wrinkling of the shock is not considered. In both cases, it would be possible to extend the model and release those constraints but this is left for future work.

SUMMARY

Starting from the Navier–Stokes equations and based on some assumptions that were checked using LES results, a stochastic ODE for the reflected-shock foot motions was presented. The general form of the governing equation relies on the assumed existence of a separation of variables, which is well supported by the LES data, allowing a transformation of what was initially a partial differential equation into an ordinary one. The derivation assumes two-dimensional motions (i.e. the spanwise wrinkling of the shock was not considered) with the shock crossing point located above the incoming boundary-layer height δ_0. Under such conditions, a governing equation for the shock-foot motions is obtained and linearised on the basis of sufficiently small shock displacements combined with the analysis of LES data. This final form of the governing equation is mathematically identical to the one postulated by Plotkin (1975), and capable of reproducing the wall-pressure low-frequency spectrum in the vicinity of the mean shock-foot position.

Upon modelling the constituents of the derived governing equation, the dynamical system can be closed and expressed in terms of its input parameters: the upstream Mach number M_1, the wedge angle θ and the upstream boundary-layer properties (i.e. skin friction and momentum thickness). Although the upstream boundary-layer properties are found to be important at setting up the interaction length, the dynamical system is mainly controlled by M_1 and θ. A wide range of input (M_1, θ) pairs was tested and the predicted most energetically significant low-frequency motions, expressed in the form of the Strouhal number S_t, were shown to remain in the range 0.01 to 0.1, confirming the experimental evidence collected in Dussauge et al. (2006). The most energetic Strouhal number was found to increase with increasing M_1 for a constant wedge angle θ, whereas it decreased with increasing wedge angle for constant M_1.

Mathematically speaking, the derived governing equation corresponds to a first-order low-pass filter and the analytical spectrum derived from forcing the system with white noise is in excellent agreement with the available experimental and numerical spectra. This result is consistent with the findings of Plotkin (1975); Poggie and Smits (2001, 2005) and leads to the suggestion that the low-frequency motions observed in SBLI need not be a characteristic of the forcing but simply the result of the low-pass filtering property of the dynamical system formed by the coupling between the boundary layer and the reflected shock, as demonstrated by the white-noise forcing. This does not mean that specific forcing from upstream (see Ganapathisubramani et al., 2007, amongst others) or downstream (see Pirozzoli and Grasso, 2006; Piponniau et al., 2009; Robinet, 2007; Touber and Sandham, 2009) does not play a role, but that they are not necessary. Obviously, if present and acting below the system cutoff frequency, they will inevitably be picked up by the system.

Further improvements to the proposed model are clearly possible and could be considered in the future: include spanwise shock wrinkling, derive better models for Δ_2, extend the derivations to compression ramps and/or hot/cold walls.

Acknowledgement The authors would like to acknowledge the UK Turbulence Consortium EP/D044073/1 for the computational time provided on the HECToR facilities, the UK's national high-performance computing service, which is provided by EPCC at the University of Edinburgh and by CCLRC Daresbury Laboratory, and funded by the Office of Science and Technology through EPSRC's High End Computing Program. We are also grateful for the financial support of the European Union through the Sixth Framework Program with the UFAST project and to the University of Southampton for the access to its high-performance computer, Iridis2.

REFERENCES

P. Dupont, C. Haddad, and J. F. Debiève. Space and time organization in a shock-induced separated boundary layer. *J. Fluid Mech.*, 559:255–277, 2006.

J.-P. Dussauge and S. Piponniau. Shock/boundary-layer interactions: possible sources of unsteadiness. *Journal of Fluids and Structures*, 24:1166–1175, 2008.

J.-P. Dussauge, P. Dupont, and J.-F. Debiève. Unsteadiness in shock wave boundary layer interaction with separation. *Aerospace Science and Technology*, 10:85–91, 2006.

B. Ganapathisubramani, N. T. Clemens, and D. S. Dolling. Effects of upstream boundary layer on the unsteadiness of shock-induced separation. *J. Fluid Mech.*, 585:369–394, 2007.

S. Piponniau, J.-P. Dussauge, J.-F. Debiève, and P. Dupont. A simple model for low-frequency unsteadiness in shock-induced separation. *J. Fluid Mech.*, 629:87–108, 2009.

S. Pirozzoli and F. Grasso. Direct numerical simulation of impinging shock wave/turbulent boundary layer interaction at $M = 2.25$. *Physics of Fluids*, 18(6), 2006.

K. J. Plotkin. Shock wave oscillation driven by turbulent boundary-layer fluctuations. *AIAA Journal 1036–1040*, 13 (8), 1975.

J. Poggie and A. J. Smits. Shock unsteadiness in a reattaching shear layer. *J. Fluid Mech.*, 429:155–185, 2001.

J. Poggie and A. J. Smits. Experimental evidence for plotkin model of shock unsteadiness in separated flow. *Physics of Fluids*, 17(1), 2005.

J.-Ch. Robinet. Bifurcations in shock-wave/laminar-boundary-layer interaction: global instability approach. *J. Fluid Mech.*, 579:85–112, 2007.

E. Touber and N. D. Sandham. Large-eddy simulation of low-frequency unsteadiness in a turbulent shock-induced separation bubble. *Theor. Comput. Fluid Dyn.*, 23:79–107, 2009.

E. Touber and N. D. Sandham. Low-order stochastic modelling of low-frequency motions in reflected shock-wave/boundary-layer interactions. *J. Fluid Mech.*, 671: 417–465, 2011.